Cellulose (2022) 29:9073–9087
https://doi.org/10.1007/s10570-022-04840-y

ORIGINAL RESEARCH

Modification of nanocellulose films in deep eutectic solvents using vinyl esters

Matias Lakovaara · Juho Antti Sirviö · Rafal Sliz · Július Vida · Tomáš Homola · Henrikki Liimatainen

Received: 14 June 2022 / Accepted: 5 September 2022 / Published online: 14 September 2022

Abstract The hydrophilicity of nanocellulose materials mitigates their good mechanical and oxygen barrier properties when exposed to humid conditions. It also limits nanocellulose use in many applications where water is present. This study reveals hydrophobic modification of cellulose nanofiber (CNF) films with vinyl esters of variable alkyl chain length using deep eutectic solvent (DES) of imidazole and triethylmethylammonium chloride as a reaction medium. Additionally, the influence of ultraviolet-ozone (UV/O_3) pretreatment on CNF film modification in DES was addressed. The esterification of CNF films in DES was proven to be a simple and fast approach to increase the hydrophobicity of the films (increasing the contact angle from 38° to 107°), requiring only a 15 min reaction time and reaction temperature of 80 °C. Moreover, the modification improved water vapor barrier properties of the films and resulted in improved mechanical properties at wet state, especially with films treated with UV and ozone before modification.

Keywords Cellulose nanofibers · Deep eutectic solvents · Esterification · Film · Vinyl esters

Introduction

Polymers derived from petroleum-based chemicals, such as polypropylene, polyethylene, polyvinyl chloride, and polyethylene terephthalate, have dominated food packaging materials for many decades. Excellent water vapor barrier and mechanical properties, low production costs, and good processability are some of the remarkable features of these plastics, which can extend the shelf life and maintain the quality of food products. However, these plastics are not biodegradable, and they still possess a low recyclability rate, a high carbon footprint, and a low oxygen barrier performance. Consequently, bio-based materials derived from lignocelluloses are an attractive option in food packaging materials because of their renewability, low toxicity, biodegradability, and abundance (Aulin et al. 2012; Peelman et al. 2016; Chi and Catchmark 2018).

Self-standing films made from cellulose nanofibers (CNFs) exhibit many appealing features and are one potential bio-based option for sustainable food

Supplementary Information The online version contains supplementary material available at https://doi.org/10.1007/s10570-022-04840-y.

M. Lakovaara · J. A. Sirviö · H. Liimatainen (✉)
Fibre and Particle Engineering Research Unit, University of Oulu, Oulu, Finland
e-mail: henrikki.liimatainen@oulu.fi

R. Sliz
Optoelectronics and Measurement Techniques Unit, University of Oulu, Oulu, Finland

J. Vida · T. Homola
Faculty of Science, Masaryk University, Brno, Czech Republic

packaging. CNF films are transparent and possess excellent barriers against oxygen and good mechanical strength in dry conditions. This is because of the high surface area of cellulose nanostrands and their inherent property to create entangled and tight networks through interfibrillar hydrogen bonds (Nair et al. 2014). CNF films can possess a tensile strength above 250 MPa and oxygen permeability below 0.1 cm^3·µm/m^2·day·atm at 50% relative humidity (RH). In comparison, most common plastics exhibit oxygen permeability between 400 and 40,000 cm^3 µm/m^2·day·atm (Henriksson et al. 2008; Aulin et al. 2010; Sehaqui et al. 2010; Lavoine et al. 2012; Wang et al. 2018; Yang et al. 2020).

CNF interacts strongly with water because of its hydrophilic characteristics, which is one of the major drawbacks preventing the use of CNF films in many food packaging applications. CNF films lose their mechanical properties, as well as oxygen and water vapor barrier performance at high humidity conditions (above 70% RH), because water molecules can break the interfibrillar hydrogen bonds and cause film swelling and structural loosening (Aulin et al. 2010; Benítez et al. 2013; Sehaqui et al. 2014; Peresin et al. 2017). Then, the gas molecules have an easier path to travel through the film, weakening oxygen and water vapor barrier properties (Nair et al. 2014; Benítez and Walther 2017).

To enhance the water resistance of CNF films, different strategies, such as direct surface modification (Rodionova et al. 2011), solvent exchange (Lavoine et al. 2012), and surface coating (Spence et al. 2011; Österberg et al. 2013b), have been reported. Because of abundant reactive hydroxy groups of cellulose, direct surface modification using different approaches, such as acetylation in liquid and gas phase (Rodionova et al. 2011, 2013), silylation, amination (Peresin et al. 2017), and reaction with fatty acids (Tomé et al. 2011), are promising routes to functionalize the surface of CNF films. One challenge with surface modification of CNF films is the passivation layer that accumulates on the film surface upon drying. Carbon-based contaminants in the air can attach onto the surface of CNF film, occupying a significant amount of the reactive hydroxy groups of cellulose. Previously, combined treatment with ultraviolet light and ozone (UV/O_3) was used to clean and activate the surface of the film before modification (Österberg et al. 2013a). The UV/O_3 treatment resulted in a higher degree of substitution in amination reaction without any substantial structural degradation of the film. Additionally, UV/O_3 activation lasted at least 2 weeks after the treatment (Österberg et al. 2013a; Peresin et al. 2017).

Another typical challenge associated with the direct surface esterification modifications of CNF films is the reaction medium. In many cases, volatile organic solvents are used for modifications, which are potentially hazardous to humans and environments. These modifications can also be complicated and slow (Sehaqui et al. 2014; Peresin et al. 2017). One promising alternative and green reaction medium for CNF film functionalization are deep eutectic solvents (DESs) (Lakovaara et al. 2021). A DES is a fluid generated by mixing and melting two compounds to form a hydrogen bond donor–acceptor pair. A characteristic feature of DES is its significantly lower melting point than its individual constituents. DESs have many appealing attributes, such as low vapor pressure, low toxicity, and biodegradability, and they can be formed from readily available low-cost chemicals. In addition, DESs can act as catalysts and reactants (Zhang et al. 2012; Smith et al. 2014).

In this study, vinyl esters with different alkyl chain lengths (3–15 carbons in the alkyl chain) were harnessed to modify the surface of CNF films using DES of imidazole and triethylmethylammonium chloride (TEMACl) as a reaction medium. The role of UV/O_3 pretreatment of the CNF films in DES-induced esterification was also elucidated. The films were characterized using attenuated total reflectance-Fourier transform infrared spectroscopy (ATR-FTIR), X-ray photoelectron spectroscopy (XPS), and field emission scanning electron microscopy (FESEM). The hydrophobicity and water barrier properties were investigated using contact angle and water vapor barrier measurements. The water absorption and mechanical properties of the films were studied in dry and wet conditions.

Experimental section

Materials

Bleached birch kraft pulp sheets were used as a cellulose raw material for nanocellulose film production after wet disintegration. Imidazole

(purity > 98.0%), TEMACl (purity > 98.0%), vinyl butyrate (stabilized with mequinol, MeHQ) (purity > 98.0%), vinyl octanoate (stabilized with MeHQ) (purity > 99.0%), vinyl laurate (stabilized with MeHQ) (purity > 99.0%), and vinyl palmitate (stabilized with MeHQ) (purity > 96.0%) were from Tokyo Chemical Industry Co. Ethanol (purity > 96%), and acetone (purity 100.0%) were from VWR International. Deionized water was used throughout the study, if not mentioned otherwise.

Preparation of cellulose nanofibers

Cellulose was mechanically nanofibrillated to CNF using a super mass colloider (Masuko, MKCA6-2, Japan). First, pulp sheets were torn apart and diluted to water, and the suspension was mixed to achieve a homogenous mixture. Then, the fibers were fed multiple times through the grinder while reducing the gap between grinding discs. The grinding procedure was described in detail by Selkälä et al. (2018). The consistency of the obtained CNF suspension was 1.7 wt.%.

Preparation of cellulose nanofiber films

CNF films were prepared by measuring 0.3 g (dry) of nanofibrillated cellulose to a beaker glass and then diluting it with water to a total weight of 110 g (0.27 wt.%). The sample was degassed through the mild ultrasonic treatment (Elmasonic P, Elma Schmidbauer GmbH, Germany) for 10 min, followed by vacuum filtration on top of the polymer membrane (Durapore DVPP 0.65 µm, Merck Millipore Ltd., Ireland) using a negative pressure of approximately 800 mbar. After the film was formed and the excess water was removed, another membrane was placed on top of the wet CNF cake. The entire system was placed between two cardboards for further vacuum drying (Karl Schröder KG, Germany) at 93 °C using a negative pressure of 900 mbar for 10 min to obtain self-standing films with a basis weight of 72.4–75.8 g/m^2. The thickness of the films varied between 46.5 and 52.8 µm as measured with a thickness gauge (FT3, Hanatek Instruments, UK) as an average of three random points.

Preparation of deep eutectic solvent

DES of imidazole and TEMACl (molar ratio of 7:3) was prepared by weighing the components into the decanting glass (total of 140 g) and heating the mixture in the oil bath at 80 °C. When approximately half of the liquid was formed, a magnetic stirrer was enabled and kept constantly mixing to speed up the formation of DES. When a clear liquid was obtained, the DES was used as a reaction medium to modify CNF films.

UV/O_3 treatment for CNF films

The UV/O_3 treatment was conducted using UVO Cleaner 42–220 (Jetlight Company Inc., USA). The device was equipped with a low-pressure mercury-vapor grid lamp, generating light at 253.7 nm with an average intensity of 28–32 mW/cm^2. The samples were illuminated from both sides for 10 min. After the UV/O_3 treatment, the samples were immediately processed further.

Modification of the CNF films in the DES

Before modification, the CNF film was washed with acetone or treated with UV/O_3 to remove possible impurities that could disturb the reaction between the reagent and cellulose film (Johansson et al. 2011; Österberg et al. 2013a). The vinyl reagent, i.e., vinyl butyrate, vinyl octanoate, vinyl laurate, or vinyl palmitate, was added into the DES and then submerged the film into the DES system horizontally. To prevent the magnetic stirrer from touching the film, a custom-made film protection design was used (Figure S24 in supporting material). The ratio between the reagent and film was 10:1 in weight. After 15 min reaction time at 80 °C, the modified film was washed four times (~5 min each time) with water to remove the DES and residues of the unreacted reagent from the film. Fresh washing liquid was used in every washing phase. Finally, the film was placed between two membranes (Durapore DVPP 0.65 µm, Merck Millipore Ltd., Ireland), which were further covered with two cardboards. Then, samples were dried in a vacuum dryer for 10 min (Karl Schröder KG, Germany).

ATR-FTIR spectroscopy

The chemical characteristics of the films were analyzed using ATR-FTIR. The spectra were recorded from small film specimens using Bruker Hyperion 3000 (USA). The wavelength range of 600–4000 cm^{-1} and a total of 32 scans at a resolution of 4 cm^{-1} were used.

X-ray photoelectron spectroscopy

The chemical composition and bonding on the surface were analyzed through XPS using the Axis Supra from Kratos Analytical Ltd (UK). The instrument uses the Al Kα spectral line with a photon energy of 1486.6 eV. An electron flood gun was used for charge compensation. The acquisition of narrow regions of the spectrum was conducted with the pass energy of 20 eV. CasaXPS software was used for the spectra analysis. The U 2 Tougaard type background was subtracted from the measured data, and mixed Gauss–Lorentzian line shapes were used for spectra fitting. The spectra were calibrated to C–C/C–H peak of C 1 s at 285 eV binding energy.

Contact angle measurements

The contact angle measurements were conducted using the DSA100 system (Krüss, Germany). The measurement system used a high-speed camera (1000 fps) to capture the drop behavior, which was consequently analyzed using drop analyzing software. A set of high-speed videos was recorded during the measurements for further analysis and contact angle extraction for various films. The Milli-Q water size of the droplet was retained at approximately 1 μL to reduce the influence of gravitational flattening. In all cases, the contact angles were extracted using the height–width method, where a rectangle enclosed by a contour line is interpreted as being the segment/part of a circle. For each sample, three measurements at different locations were conducted. The acquired results were averaged, and the standard deviations were calculated.

Water vapor permeability

Water vapor permeability (WVP) of the films was determined according to ASTM Standard E96/E96M. All films were conditioned in a separate room with controlled conditions (23 °C ± 1 °C and 50% ± 2.5% RH) for 48 h, and then the measurements were conducted in the same conditions (room was equipped with a fan to ensure good circulation of air inside the room). The test sample was put between 100 mL Schott Duran© glass bottle and a cap with a hole (area of 5 cm^2) drill on it. The glass bottle was filled with water one-fourth of its volume, and a rubber seal was used to ensure a tight sealing. Weight loss of the bottles was recorded at 1 h intervals for 8 h in the course of 2 days. A weight loss–time curve was drawn, the slope of the strain hardening region was estimated, and the water vapor transmission rate (WVTR) was determined by dividing the slope by the exposed film area. WVP was calculated as follows:

$$\mathrm{WVP} = (\mathrm{WVTR}/\mathrm{S} * (\mathrm{R}_1 - \mathrm{R}_2)) * \mathrm{h} \quad (1)$$

where S is the saturation vapor pressure at the test temperature (2800 Pa at 23 °C), R_1 is the RH in the bottle expressed as a fraction (1), R_2 is the RH in the room expressed as a fraction (0.5), and h is the thickness of the film sample.

Moisture absorption measurements

Moisture absorption measurements were conducted by weighing small film specimens in 0% and 100% RH and recording the weight value of three separate specimens of each sample. For 0% RH, the samples were dried and kept in a desiccator to absorb moisture in the silica gel. For 100% RH, the samples were kept in a desiccator, where water-absorbing silica gel was replaced with water. Cumulative weight percentage increase of the specimens was calculated, and the results were reported as an average of three measurements per film.

Mechanical properties

Mechanical properties of the films were measured using a universal testing machine (Zwick Roell, Ulm, Germany) with a 2 kN load cell. The samples were prepared by cutting five to seven strips from each film with a width of 5 mm and length of 50–70 mm. The test was conducted in 50% RH with fully wetted samples at the wet state. The films were kept in a separate room with controlled conditions (23 °C ± 1 °C

and 50% ± 2.5% RH) 48 h before analysis. For the wet state tensile measurements, the strips were immersed in water 1 h before analysis, and excess water was swept with tissue paper before testing. Before mechanical tests, the thickness of the strips was measured as an average of three random measuring points using a thickness gauge (FT3, Hanatek Instruments, UK). For tensile testing, the gauge length was set to 40 mm, and the strain was controlled with a speed of 5 mm/min with a prestrain value of 0.1 and 1 MPa for dry and wet films, respectively. Young's modulus was calculated from the slope of the line from the linear region of the stress–strain curve, and an ultimate tensile strength was determined as the stress of specimen fracture. For dry tensile measurements (50% RH), the results are reported as an average of five tests and an average of three tests for wet tensile measurements.

SEM imaging

FESEM (JEOL JSM-7900F, Japan) was used to study the surface and cross-section morphologies of the films. Images were taken at an accelerating voltage of 5.0 kV. The samples were sputtered with platinum (High-Resolution Sputter Coater, Agar Scientific, UK) before analysis using a sputtering time of 30 s and a current of 40 mA.

Results and discussion

Chemical characteristics of CNF films

CNF films were modified with vinyl esters with different alkyl chain lengths using a DES of imidazole and TEMACl (molar ratio of 7:3) as a reaction medium. Four different vinyl esters, i.e., vinyl butyrate (three carbons in alkyl chain), vinyl octanoate (seven carbons in alkyl chain), vinyl laurate (11 carbons in alkyl chain), or vinyl palmitate (15 carbons in alkyl chain), were used. The modified films are named based on the vinyl ester used. Additionally, the role of film pretreatment in DES-mediated esterification reaction was revealed, i.e., films were washed with acetone or treated with UV/O_3 before modification (labeled as UV/O_3 treated films). Pure CNF film and UV/O_3 treated CNF film served as reference films.

In this study DES was used as a reaction medium and imidazole in DES could act as catalyst via formation of acyl imidazole with vinyl esters (Pires et al. 2015). DES based on imidazole and TEMACl was harnessed as it bears no similar chemical groups compared to cellulose (i.e. hydroxy groups) which could react with esterification agent (i.e. vinyl ester). Previously, pyridine has been used a reaction medium for cellulose modification, but pyridine is more volatile than the imidazole of the DES used in this study (vapor pressure of pyridine and imidazole are 2.4 kPa at 20 °C and 0.3 Pa at 20 °C, respectively). CNF films have been esterified using fatty acid chlorides, but their drawback is a long reaction time (90 min) and high reaction temperature (110 °C). In addition, fatty acid chlorides are more harmful than vinyl esters used in this study (Nawaz et al. 2013; Hinner et al. 2016; Balasubramaniam et al. 2020). Other esterification reagents have been studied, but most of them are utilized in homogenous media with solvent such as ionic liquid. However, dissolution of cellulose by ionic liquids prevents their use in current application (Kakko et al. 2017; Kostag et al. 2019).

The reaction between vinyl esters and hydroxy groups of cellulose occurred through an esterification route (Fig. 1). ATR-FTIR spectroscopy was used to analyze the chemical structure of the reacted films in terms of ester bond formation and elucidate the effect of UV/O_3 treatment on the modification. Figure 2 shows the ATR-FTIR spectra of pristine CNF and laurate-modified films and their UV/O_3-treated counterparts. The spectra of the other samples are presented in supporting material in Figure S1. Compared

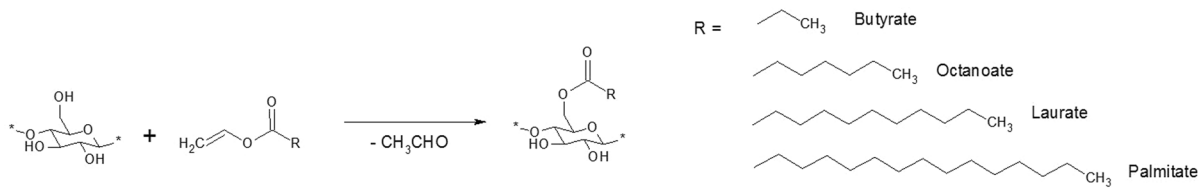

Fig. 1 Schematic representation of the esterification reaction between vinyl esters and hydroxy groups of cellulose

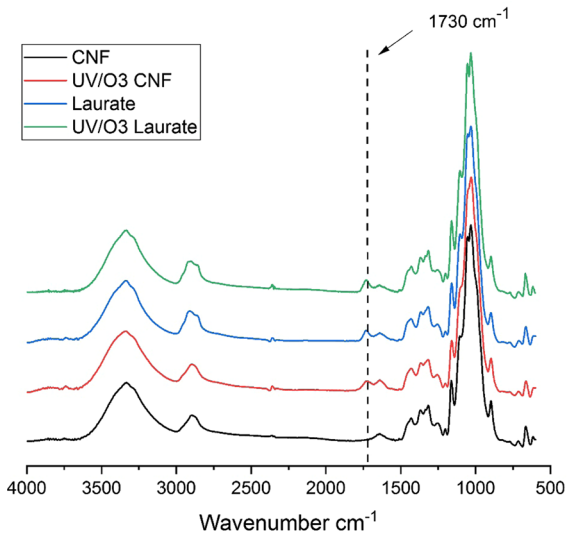

Fig. 2 ATR-FTIR spectra of pristine CNF and laurate modified films and their UV/O_3-treated counterparts. The dashed line corresponds to the peak of the O–C=O ester bond at a wavenumber of 1730 cm^{-1}

with reference CNF film, the modified films showed a new peak at a wavenumber of 1730 cm^{-1}, indicating the presence of O–C=O bond of the ester group and a successful esterification reaction of CNF film in the DES medium. Unexpectedly, the ester peak was not found with a reaction of vinyl palmitate using the UV/O_3-pretreated CNF film despite multiple attempts (Figure S1). This could be because of a low degree of substitution of the sample (see Table 1) or low resolution of ATR-FTIR. Later, it was clearly confirmed with contact angle measurements and XPS analysis that the reaction also occurred with vinyl palmitate.

The UV/O_3-pretreated CNF film showed a carbonyl peak similar to the modified films without adding any vinyl reagent. Ozone is a very powerful oxidation agent; therefore, it can introduce carboxylic acid or carbonyl groups at the material surfaces. Ozone mainly oxidizes the primary hydroxy group of cellulose, yet simultaneously secondary hydroxy groups can be oxidized. Ozone can also results in cleavage of glycosidic bonds between cellulose molecules. Typically, carbonyl groups are seen in ozone-treated polymer films in the 1700–1750 cm^{-1} region (Hedenberg and Gatenholm 1996; Romero-Sánchez et al. 2005; Österberg et al. 2013a; Wen et al. 2020). Here the carbonyl peak was observed at a wavenumber of 1730 cm^{-1}; otherwise, the spectra of CNF and UV/O_3 CNF samples remained unchanged.

Furthermore, XPS analysis was conducted to support the findings from ATR-FTIR spectroscopy and further characterize the surface chemical composition of the CNF films. Table 1 presents the elemental concentration of carbon, oxygen, and nitrogen, and concentration of carbon bonds (XPS survey spectra and C1s deconvolution spectra of CNF, butyrate, laurate, and UV/O_3-treated counterparts are presented in supporting information in Figures S2–S7 and S8–S13, respectively. A full table of elemental concentration of the samples is presented in Table S1). All esterified films modified in DES exhibit a higher O–C=O bond concentration (2.3–4.2%) than the original CNF film (O–C=O bond concentration of 2.0%), supporting the findings from ATR-FTIR measurements about the successful esterification reaction. In alignment with

Table 1 XPS elemental concentrations of carbon, oxygen, and nitrogen, and concentration of carbon bonds for the reference, UV/O_3 pretreated, and esterified CNF films

	Elemental concentration (%)			Concentration of carbon bonds (%)			
Sample	C 1s	O 1s	N 1s	C–C	C–O	O–C–O	O–C=O
CNF	67.0	31.6	0.6	28.7	55.4	13.90	2.0
UV/O_3 CNF	61.9	34.8	0.6	24.2	56.0	16.7	3.1
Butyrate	63.5	36.3	0.0	17.8	62.5	15.4	4.2
UV/O_3 Butyrate	64.9	35.0	0.1	19.7	61.1	15.0	4.2
Octanoate	65.9	33.8	0.2	23.6	58.2	14.2	4.1
UV/O_3 Octanoate	66.3	33.3	0.0	24.8	57.2	14.2	3.8
Laurate	64.9	35.0	0.1	19.6	62.1	15.4	2.8
UV/O_3 Laurate	64.9	35.0	0.0	21.5	60.3	14.8	3.4
Palmitate	67.1	32.7	0.2	27.2	56.5	13.8	2.5
UV/O_3 Palmitate	66.0	33.3	0.4	24.9	58.2	14.6	2.3

these results, the C–C bond concentration of the DES-modified films (17.8%–27.2%) decreased more than the reference CNF film (28.7%).

The O–C=O bonds in pristine CNF film likely originate from the hemicelluloses of the pulp, or the bonds can be formed during the pulping and bleaching processes since the unmodified cellulose does not contain these bonds (Bayer et al. 2016). Additionally, the UV/O_3-treated CNF film exhibits a higher O–C=O bond concentration (3.1%) than the original CNF film, supporting the FTIR results of CNF oxidation. The oxidation of lignin on the pulp surface was earlier seen in the XPS data as a decrease in the C–C bond and an increase in the O–C=O bond concentration (Koljonen et al. 2003). Similarly, the C–C bond concentration decreased from 11 to 4%, and O–C=O bond concentration increased (percentages not reported) after treating CNF film samples with UV/O_3 (Österberg et al. 2013a). This result is consistent with our results showing that UV/O_3-treated CNF film had a lower C–C bond concentration (24.2%) than the original CNF film (28.7%) and a higher O–C=O bond concentration (3.1% and 2.0%).

The O–C=O bond concentration decreased as a function of the alkyl chain length of the vinyl reagent. Vinyl butyrate with the shortest carbon chain resulted in the O–C=O bond concentration of 4.2%, whereas vinyl palmitate had an O–C=O bond concentration of 2.5%. This suggests that the reaction rate decreased with increasing alkyl chain length. A similar trend has previously been reported in the literature (Leszczyńska et al. 2018).

The UV/O_3 pretreatment of the CNF films increased the reaction efficiency of esterification only with vinyl laurate (O–C=O bond concentration with and without UV/O_3 was 3.4 and 2.8%, respectively). With vinyl butyrate, UV/O_3 treatment had no effect on O–C=O concentration, while it decreased with vinyl octanoate and palmitate after the UV/O_3 treatment.

XPS analysis was also used to elucidate whether the DES medium reacted with the films or there were any traces of the DES remaining in the films. The films were revealed in terms of their nitrogen content as both DES components, i.e., imidazole and TEMACl, contain nitrogen in their structure. Both the pristine CNF and UV/O_3-treated films exhibited 0.6% nitrogen content, whereas the DES-modified samples had a nitrogen amount ranging from 0.0 to 0.4% (Table 1). Therefore, the DES modification decreased the amount of nitrogen, suggesting that DES did not react with the films or there were not any DES traces left in the films. These findings are consistent with our previous experiments (Lakovaara et al. 2021).

The influence of esterification in DES and UV/O_3 treatment on the structure and morphology of the films was investigated through FESEM imaging. Figure 3 shows the surface (a–d) and cross-sectional FESEM images (e–h) of the pristine CNF, UV/O_3 CNF, butyrate, and UV/O_3 butyrate (FESEM images of other samples are presented in supporting information Figure S14–S23). Based on the images, the DES modification or UV/O_3 treatment did not affect the visual appearance of the films, and all films possessed a tightly packed and nonporous structure. The previous results also support that UV/O_3 treatment does not degrade the CNF film despite the strong oxidation efficiency of ozone (Österberg et al. 2013a). However, the UV-treated and DES-modified films have less rough surface structure than non-UV-treated and DES-modified films. Moreover, all cross-sectional images (Fig. 2e–h) display a typical layered structure of CNF films.

Contact angle of the films

The role of esterification and UV/O_3 pretreatment in the alteration of surface characteristics of the films was evaluated through contact angle measurements (Fig. 4). All DES-modified films exhibit higher contact angles (77.0°–106.5°) than unmodified reference CNF film (37.8°); thus, the esterification increased the hydrophobicity of the films. These contact angles are substantially higher than those obtained previously with CNF films modified using n-octylsuccinic anhydride in DES of imidazole and TEMACl, where the film exhibited a contact angle of 51° (Lakovaara et al. 2021). The highest contact angle was obtained with the UV/O_3-treated and vinyl laurate-reacted film with a contact angle of 106.5°. Among non-UV/O_3-treated films, vinyl octanoate resulted in the highest contact angle of 94.7°.

The UV/O_3 treatment was conducted to clean and enhance the reactivity of the surface of the CNF films. When CNF films are exposed to air upon drying, carbonaceous contamination layers accumulate to the highly hydrophilic CNF surface (Johansson et al. 2011; Österberg et al. 2013a). The UV/O_3

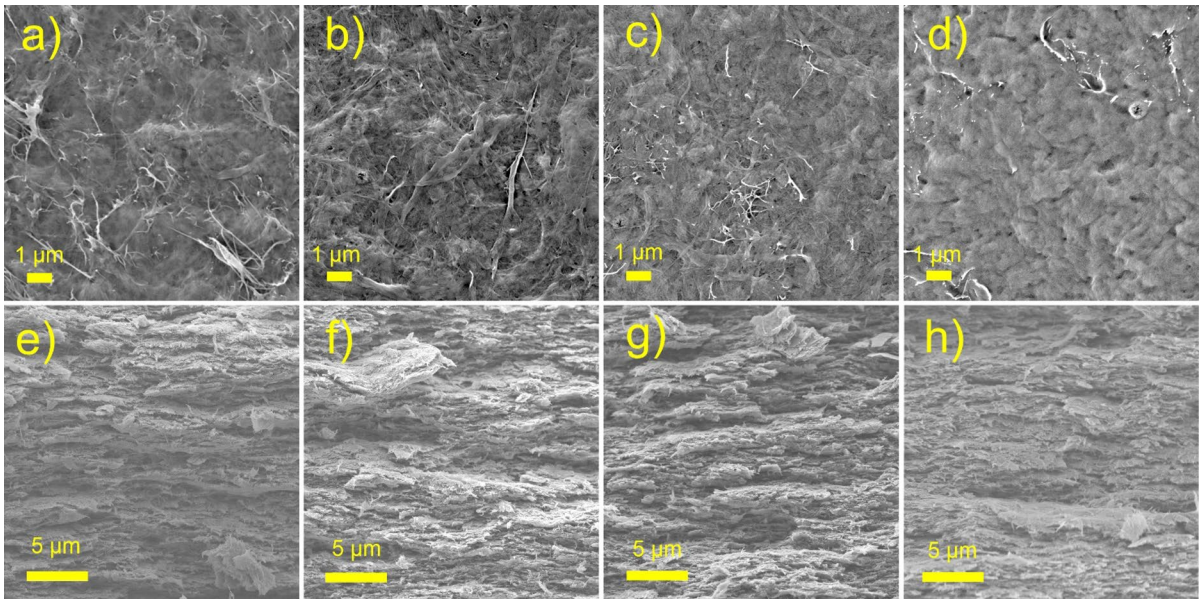

Fig. 3 FESEM surface (**a**–**d**) and cross-sectional (**e**–**h**) images of the films. **a** and **e** CNF, **b** and **f** UV/O3 CNF, **c** and **g** butyrate, and **d** and **h** UV/O_3 butyrate

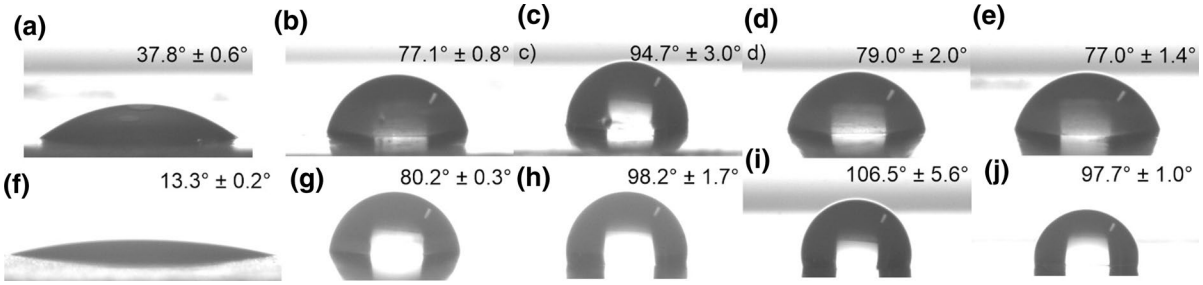

Fig. 4 Film samples at the start of the contact angle measurements. On the top row are non-UV/O_3-treated samples **a** CNF, **b** butyrate, **c** octanoate, **d** laurate, and **e** palmitate; below **f**–**j** are their UV/O_3-treated counterparts

treatment can remove carbon-based impurities and attach carboxylic acid or carbonyl groups at the material surfaces, thus making the films more hydrophilic (Österberg et al. 2013a). Supporting these previous findings, the contact angle of UV/O_3-treated CNF film was very low (13.3°), significantly lower than the reference CNF film (37.8°). For all DES-modified films, the UV/O_3 treatment increased the contact angle. With the films reacted with shorter alkyl chains, i.e., vinyl butyrate and octanoate, the contact angle increase was only a few degrees (for butyrate from 77.1° to 80.2° and octanoate from 94.7° to 98.2°). Meanwhile, the increase was more significant with longer alkyl chain samples (laurate and palmitate). The contact angle increased from 79.0° to 106.5° and 77.0° to 97.7° with laurate and palmitate, respectively.

The contact angle value seems to be affected by at least two factors: the length of the alkyl chain and reaction rate (i.e., the O–C=O bond content; see Table 1) (Leszczyńska et al. 2018). For example, butyrate has a higher reaction rate (4.24%) than palmitate (2.47%); however, the contact angles are the same (77°). Octanoate had a slightly lower reaction rate (4.05%) than butyrate, but a longer alkyl chain length of vinyl octanoate resulted in a higher contact

angle of 94.7°. Laurate had a lower reaction rate (2.82%) than octanoate, with a contact angle of 79.0° despite a longer carbon chain length. The influence of the UV and ozone pretreatment on improvement in reaction rate was noted with vinyl laurate, which also increased its contact angle.

Water vapor barrier performance of the films

Figure 5 shows the water vapor permeabilities of the films. The reference CNF film exhibited the highest (i.e. the worst value) WVP of 18.67 g·µm/m^2·d·kPa, whereas all the other films had a lower WVP ranging from 14.36 to 18.11 g·µm/m^2·d·kPa, which is consistent with results reported in the literature (Wang et al. 2018). The UV/O_3-pretreated CNF film presented a WVP value of 15.68 g·µm/m^2·d·kPa, which is second highest of the UV-treated samples. The lowest value (i.e., the best value) was with octanoate sample with 14.36 g·µm/m^2·d·kPa.

Water vapor transmission through the film depends on many factors, such as film thickness, density, porosity, crystallinity, and hydrophobicity. Water vapor penetrates through the film in a multistep diffusion process where water molecules adsorb on the surface of the film first, then diffuse through the film, and finally evaporate from the surface of the film (Chi and Catchmark 2018). The enhanced WVP of the UV/O_3-treated film might be attributed to the cross-linking promoted by the carbonyl and carboxyl groups. These bonds can probably resist better the bond breakage induced by the moisture than the hydrogen bonds between pristine cellulose chains (Klein et al. 2008; Torres et al. 2010). Similar to contact angle values, the influence of the UV/O_3 treatment on WVP was observed with samples modified with short alkyl chain samples, i.e., butyrate and octanoate.

Moisture absorption of the films

Figure 6 shows the cumulative moisture absorption of the films in the 0–100% RH range. All UV/O_3-treated films displayed a lower moisture absorption than their nonpretreated counterparts. The lowest moisture absorption was with UV/O_3 butyrate with a 16.6 wt.% weight increase, and the second-lowest was with UV/O_3 CNF with a 17.8 wt.% weight

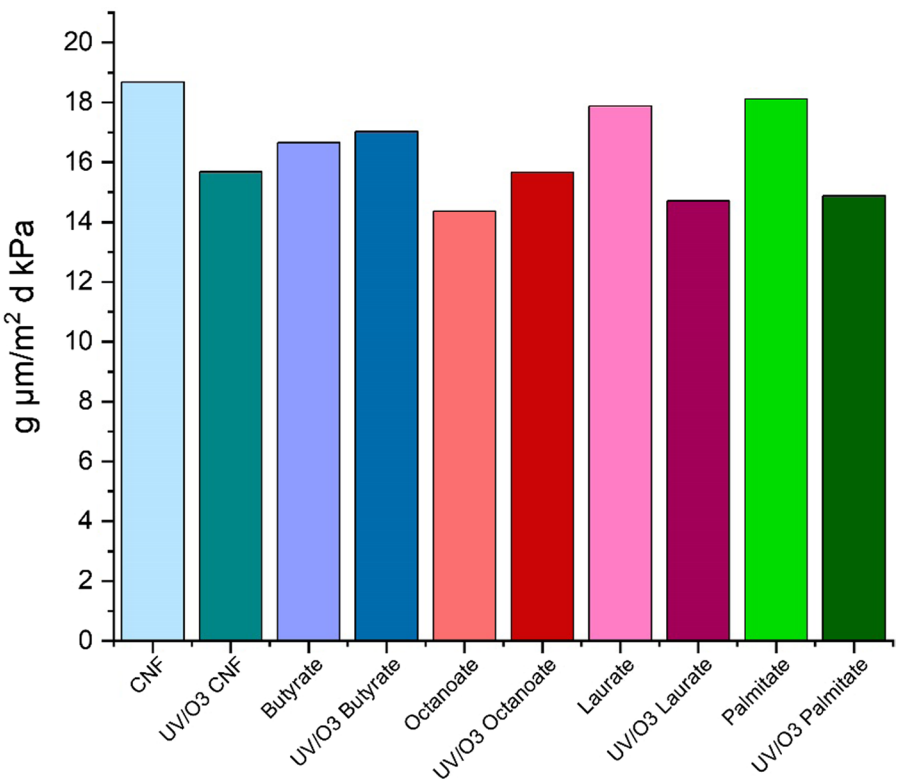

Fig. 5 Water vapor permeability of the films

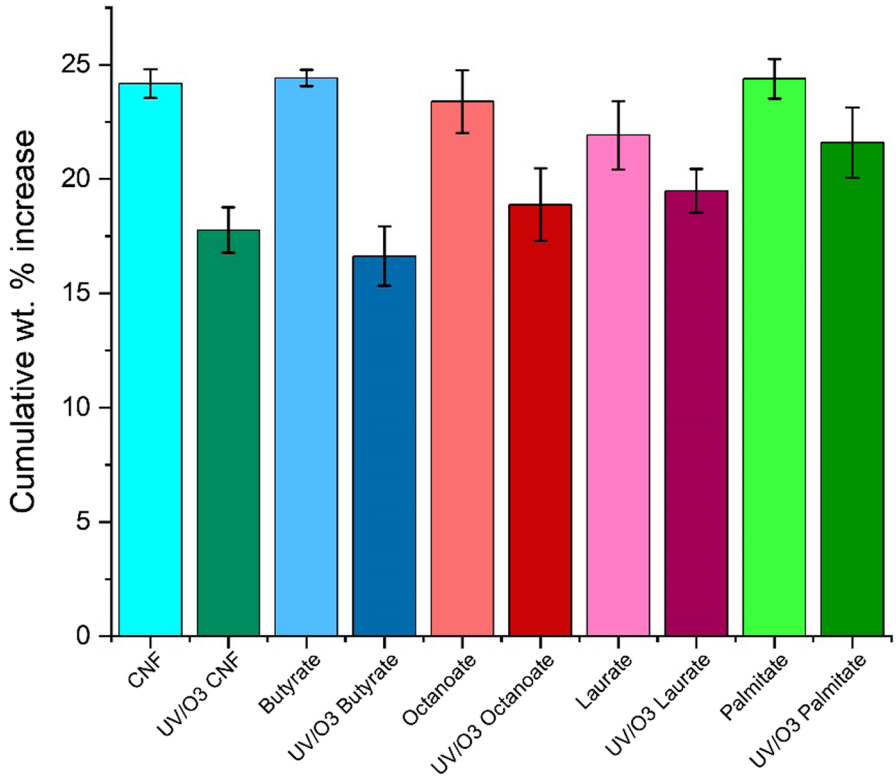

Fig. 6 Cumulative water vapor absorption of the films from 0 to 100% RH

increase. For other UV/O_3-treated films, the moisture absorption increased as the function of alkyl chain length. For non-UV/O_3-treated samples, the values were close to each other, i.e., laurate had the lowest moisture absorption of 21.9 wt.%, whereas the other films exhibited moisture absorption between 23.4 and 24.4%. Overall, the moisture absorption was presumably associated with the interfibrillar bonding of CNFs as the UV/O_3 can promote the cross-linking, whereas the hydrogen bonding reduces as the alkyl chain length increases (Torres et al. 2010).

Mechanical properties of the films

Mechanical properties of the films were evaluated using a tensile test in 50% RH and wet state. Figure 7 shows the stress–strain curves of the films. Table 2 summarizes the tensile strength (at break), strain, and modulus values. The original CNF film had the highest tensile strength of 175 MPa at 50% RH, and all esterified films without UV/O_3 treatment displayed a slightly lower tensile strength ranging from 158 to 171 MPa, similar to the values reported in the literature (Henriksson et al. 2008; Klemm et al. 2011; Lindström 2017). The UV/O_3 treatment slightly reduced the film strength with almost all samples. This reduction in strength properties may be attributed to the oxidation of cellulose and further breakage of interfibrillar hydrogen bonds, as noted earlier (Taniguchi and Okamura 1998; Torres et al. 2010; Österberg et al. 2013a; Benítez et al. 2013).

The esterification improved the strength properties of the films at the wet state as the original CNF film displayed the lowest tensile strength of 9.6 MPa. Meanwhile, the modified films possessed a wet tensile strength between 11.5 and 18.9 MPa. This improved wet tensile strength was more pronounced with samples modified with a longer alkyl chain length, i.e., laurate and palmitate. The tensile strengths and modulus were further increased at the wet state when the films were exposed with the UV/O_3 treatment. However, these samples were stiffer, and they presented lower strain values. This phenomenon is seen from Fig. 7b, where stress–strain curves of the UV/O_3-treated samples are separated from those of non-UV/O_3-treated ones. Overall, the UV/O_3 palmitate exhibited the highest wet tensile strength of 18.9 MPa. Unexpectedly, the UV/

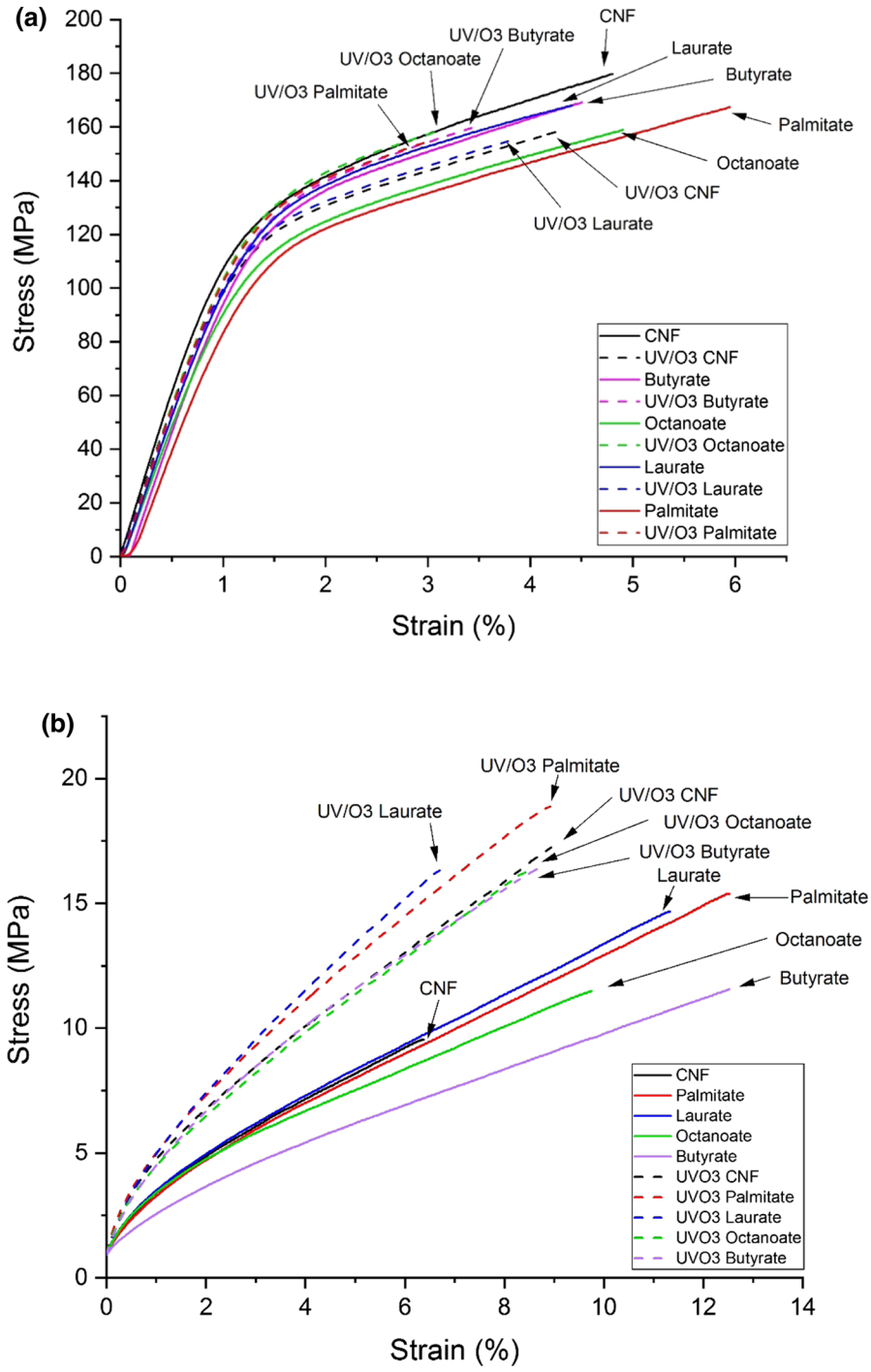

Fig. 7 Stress–strain curves of the films at **a** 50% RH and **b** wet state. The solid lines indicate untreated films, whereas the dashed lines indicate UV/O_3-treated films

O_3-treated CNF film had the second-highest tensile strength of 17.6 MPa at wet state, which can be attributed to the UV/O_3-induced cross-linking (Torres et al. 2010) and decrease in the amount of hydroxy groups.

Water had a significant impact on the films since wet films had a notable lower tensile strength and Young's modulus and increased strain than dry films. This behavior is very common for nanocellulose films since water breaks the internal hydrogen bonds and

Table 2 Mechanical properties of the films at 50% RH and wet state

50% Sample	Tensile strength (MPa)	Strain (%)	Modulus (GPa)
CNF	175 ± 11	5.2 ± 0.7	11.1 ± 0.6
UV/O_3 CNF	161 ± 6	4.9 ± 0.6	10.7 ± 0.3
Butyrate	171 ± 10	4.9 ± 0.4	10.8 ± 0.5
UV/O_3 Butyrate	160 ± 5	3.6 ± 0.4	11.3 ± 0.2
Octanoate	158 ± 5	4.8 ± 0.5	10.2 ± 0.1
UV/O_3 Octanoate	160 ± 7	3.2 ± 0.4	11.5 ± 0.2
Laurate	163 ± 11	4.8 ± 0.8	10.5 ± 0.4
UV/O_3 Laurate	155 ± 8	4.1 ± 0.5	10.8 ± 0.3
Palmitate	168 ± 11	5.0 ± 0.8	10.8 ± 0.4
UV/O_3 Palmitate	160 ± 8	3.5 ± 0.7	11.4 ± 0.146
Wet Sample	Tensile strength (MPa)	Strain (%)	Modulus (MPa)
CNF	9.6 ± 0.2	6.6 ± 0.2	302 ± 18
UV/O_3 CNF	17.6 ± 1.2	8.4 ± 1.1	529 ± 43
Butyrate	11.9 ± 0.6	12.55 ± 0.05	185 ± 14
UV/O_3 Butyrate	16.8 ± 0.2	9.0 ± 1.5	437 ± 27
Octanoate	11.5 ± 0.2	9.4 ± 0.3	313 ± 6
UV/O_3 Octanoate	16.4 ± 0.4	6.7 ± 1.3	527 ± 53
Laurate	14.9 ± 0.7	10.3 ± 1.1	302 ± 14
UV/O_3 Laurate	16.7 ± 0.4	7.4 ± 0.5	519 ± 13
Palmitate	15.4 ± 0.9	12.0 ± 0.4	282 ± 15
UV/O_3 Palmitate	18.9 ± 0.3	7.8 ± 1.0	525 ± 29

promotes interfibrillar slippage. These factors allow the film stretch better under stress (Benítez et al. 2013; Sehaqui et al. 2014; Benítez and Walther 2017). The effect of water on the films is also displayed by the stress–strain curves. The stress–strain curves at wet conditions contain a short or nonexistent linear elastic region, and the curve transforms straight into a strain hardening region (Sethi et al. 2019).

Conclusions

A straightforward and fast modification of CNF films with vinyl esters using the DES of imidazole and TEMACl as a reaction medium was successfully developed. The reaction was conducted at mild conditions; a reaction time and temperature of approximately 15 min and 80 °C were required. The role of UV/O_3 pretreatment on the esterification of CNF films was also revealed. The DES-induced esterification increased the contact angles of all films. This phenomenon was further promoted when the films were pretreated with the UV/O_3. All modified films exhibited better water vapor barrier properties than the pristine CNF film; however, UV/O_3 treatment only slightly enhanced the water barrier properties of some DES-modified films. At dry state, all modified films exhibited slightly lower tensile strength than the reference film. However, a significant increase in mechanical properties was observed at the wet state with the film pretreated with UV/O_3. Additionally, UV/O_3-treated films exhibited a lower moisture absorption uptake than non-UV/O_3-treated films.

Electronic supplementary information

ATR-FTIR spectra of Butyrate, Octanoate, Palmitate samples and their UV/O_3 treated counterparts. Full

table of XPS results. XPS survey spectra and C1 convolution spectra of CNF, butyrate, laurate and their UV/O_3 treated counterparts. FESEM surface and cross-sectional images of other samples. A custom-made film protection design.

Acknowledgments The authors acknowledge the support from the Academy of Finland project "ACNF" (325276) and the CzechNanoLab Research Infrastructure supported by MEYS CR (LM2018110). FESEM imaging was conducted with the support of the Centre for Material Analysis, University of Oulu, Finland. We gratefully thank the help of our laboratory staff.

Author contributions ML: conceptualization, investigation, writing—original draft. JS: conceptualization, writing—review and editing. RS: investigation, writing—original draft. JV: investigation, writing—original draft. TH: writing—review and editing. HL: writing—review and editing, project administration, funding acquisition, supervision.

Funding Open Access funding provided by University of Oulu including Oulu University Hospital. The research was supported by the Academy of Finland project "ACNF" (325276) and the CzechNanoLab Research Infrastructure supported by MEYS CR (LM2018110).

Data availability All authors declare that all data and materials support their published claims and comply with field standards.

Declarations

Conflict of interest The authors declare they have no competing or financial interests.

Consent for publication All authors have given approval to the final version of the manuscript.

References

Aulin C, Gällstedt M, Lindström T (2010) Oxygen and oil barrier properties of microfibrillated cellulose films and coatings. Cellulose 17:559–574. https://doi.org/10.1007/s10570-009-9393-y

Aulin C, Salazar-Alvarez G, Lindström T (2012) High strength, flexible and transparent nanofibrillated cellulose–nanoclay biohybrid films with tunable oxygen and water vapor permeability. Nanoscale 4:6622. https://doi.org/10.1039/c2nr31726e

Balasubramaniam SL, Patel AS, Nayak B (2020) Surface modification of cellulose nanofiber film with fatty acids for developing renewable hydrophobic food packaging. Food Packag Shelf Life 26:100587. https://doi.org/10.1016/j.fpsl.2020.100587

Bayer T, Cunning BV, Selyanchyn R et al (2016) High temperature proton conduction in nanocellulose membranes: paper fuel cells. Chem Mater 28:4805–4814. https://doi.org/10.1021/acs.chemmater.6b01990

Benítez AJ, Torres-Rendon J, Poutanen M, Walther A (2013) Humidity and multiscale structure govern mechanical properties and deformation modes in films of native cellulose nanofibrils. Biomacromol 14:4497–4506. https://doi.org/10.1021/bm401451m

Benítez AJ, Walther A (2017) Cellulose nanofibril nanopapers and bioinspired nanocomposites: a review to understand the mechanical property space. J Mater Chem A 5:16003–16024. https://doi.org/10.1039/C7TA02006F

Chi K, Catchmark JM (2018) Improved eco-friendly barrier materials based on crystalline nanocellulose/chitosan/carboxymethyl cellulose polyelectrolyte complexes. Food Hydrocoll 80:195–205. https://doi.org/10.1016/j.foodhyd.2018.02.003

Hedenberg P, Gatenholm P (1996) Conversion of plastic/cellulose waste into composites. II. Improving adhesion between polyethylene and cellulose using ozone. J Appl Polym Sci 60:2377–2385. https://doi.org/10.1002/(SICI)1097-4628(19960627)60:13%3c2377::AID-APP9%3e3.0.CO;2-B

Henriksson M, Berglund LA, Isaksson P et al (2008) Cellulose nanopaper structures of high toughness. Biomacromol 9:1579–1585. https://doi.org/10.1021/bm800038n

Hinner LP, Wissner JL, Beurer A et al (2016) Homogeneous vinyl ester-based synthesis of different cellulose derivatives in 1-ethyl-3-methyl-imidazolium acetate. Green Chem 18:6099–6107. https://doi.org/10.1039/C6GC02005D

Johansson L-S, Tammelin T, Campbell JM et al (2011) Experimental evidence on medium driven cellulose surface adaptation demonstrated using nanofibrillated cellulose. Soft Matter 7:10917. https://doi.org/10.1039/c1sm06073b

Kakko T, King AWT, Kilpeläinen I (2017) Homogenous esterification of cellulose pulp in [DBNH][OAc]. Cellulose 24:5341–5354. https://doi.org/10.1007/s10570-017-1521-5

Klein RJ, Fischer DA, Lenhart JL (2008) Systematic oxidation of polystyrene by ultraviolet-ozone, characterized by near-edge X-ray absorption fine structure and contact angle.

Langmuir 24:8187–8197. https://doi.org/10.1021/la800134u

Klemm D, Kramer F, Moritz S et al (2011) Nanocelluloses: a new family of nature-based materials. Angew Chem Int Ed 50:5438–5466. https://doi.org/10.1002/anie.201001273

Koljonen K, Österberg M, Johansson L-S, Stenius P (2003) Surface chemistry and morphology of different mechanical pulps determined by ESCA and AFM. Colloids Surf, A 228:143–158. https://doi.org/10.1016/S0927-7757(03)00305-4

Kostag M, Gericke M, Heinze T, El Seoud OA (2019) Twenty-five years of cellulose chemistry: innovations in the dissolution of the biopolymer and its transformation into esters and ethers. Cellulose 26:139–184. https://doi.org/10.1007/s10570-018-2198-0

Lakovaara M, Sirviö JA, Ismail MY et al (2021) Hydrophobic modification of nanocellulose and all-cellulose composite films using deep eutectic solvent as a reaction medium. Cellulose 28:5433–5447. https://doi.org/10.1007/s10570-021-03863-1

Lavoine N, Desloges I, Dufresne A, Bras J (2012) Microfibrillated cellulose—its barrier properties and applications in cellulosic materials: a review. Carbohyd Polym 90:735–764. https://doi.org/10.1016/j.carbpol.2012.05.026

Leszczyńska A, Stafin K, Pagacz J et al (2018) The effect of surface modification of microfibrillated cellulose (MFC) by acid chlorides on the structural and thermomechanical properties of biopolyamide 4.10 nanocomposites. Ind Crops Prod 116:97–108. https://doi.org/10.1016/j.indcrop.2018.02.022

Lindström T (2017) Aspects on nanofibrillated cellulose (NFC) processing, rheology and NFC-film properties. Curr Opin Colloid Interface Sci 29:68–75. https://doi.org/10.1016/j.cocis.2017.02.005

Nair SS, Zhu J, Deng Y, Ragauskas AJ (2014) High performance green barriers based on nanocellulose. Sustain Chem Process 2:23. https://doi.org/10.1186/s40508-014-0023-0

Nawaz H, Pires PAR, El Seoud OA (2013) Kinetics and mechanism of imidazole-catalyzed acylation of cellulose in LiCl/N, N-dimethylacetamide. Carbohyd Polym 92:997–1005. https://doi.org/10.1016/j.carbpol.2012.10.009

Österberg M, Peresin MS, Johansson L-S, Tammelin T (2013a) Clean and reactive nanostructured cellulose surface. Cellulose 20:983–990. https://doi.org/10.1007/s10570-013-9920-8

Österberg M, Vartiainen J, Lucenius J et al (2013b) A fast method to produce strong NFC films as a platform for barrier and functional materials. ACS Appl Mater Interfaces 5:4640–4647. https://doi.org/10.1021/am401046x

Peelman N, Ragaert P, Verguldt E et al (2016) Applicability of biobased packaging materials for long shelf-life food products. Packaging Research. https://doi.org/10.1515/pacres-2016-0002

Peresin MS, Kammiovirta K, Heikkinen H et al (2017) Understanding the mechanisms of oxygen diffusion through surface functionalized nanocellulose films. Carbohyd Polym 174:309–317. https://doi.org/10.1016/j.carbpol.2017.06.066

Pires PAR, Malek NI, Teixeira TC et al (2015) Imidazole-catalyzed esterification of cellulose in ionic liquid/molecular solvents: a multi-technique approach to probe effects of the medium. Ind Crops Prod 77:180–189. https://doi.org/10.1016/j.indcrop.2015.08.015

Rodionova G, Hoff B, Lenes M et al (2013) Gas-phase esterification of microfibrillated cellulose (MFC) films. Cellulose 20:1167–1174. https://doi.org/10.1007/s10570-013-9887-5

Rodionova G, Lenes M, Eriksen Ø, Gregersen Ø (2011) Surface chemical modification of microfibrillated cellulose: improvement of barrier properties for packaging applications. Cellulose 18:127–134. https://doi.org/10.1007/s10570-010-9474-y

Romero-Sánchez MD, Mercedes Pastor-Blas M, Martín-Martínez JM, Walzak MJ (2005) Addition of ozone in the UV radiation treatment of a synthetic styrene-butadiene-styrene (SBS) rubber. Int J Adhes Adhes 25:358–370. https://doi.org/10.1016/j.ijadhadh.2004.12.001

Sehaqui H, Liu A, Zhou Q, Berglund LA (2010) Fast preparation procedure for large, flat cellulose and cellulose/inorganic nanopaper structures. Biomacromol 11:2195–2198. https://doi.org/10.1021/bm100490s

Sehaqui H, Zimmermann T, Tingaut P (2014) Hydrophobic cellulose nanopaper through a mild esterification procedure. Cellulose 21:367–382. https://doi.org/10.1007/s10570-013-0110-5

Selkälä T, Suopajärvi T, Sirviö JA et al (2018) Rapid uptake of pharmaceutical salbutamol from aqueous solutions with anionic cellulose nanofibrils: the importance of pH and colloidal stability in the interaction with ionizable pollutants. Chem Eng J 350:378–385. https://doi.org/10.1016/j.cej.2018.05.163

Sethi J, Visanko M, Österberg M, Sirviö JA (2019) A fast method to prepare mechanically strong and water resistant lignocellulosic nanopapers. Carbohyd Polym 203:148–156. https://doi.org/10.1016/j.carbpol.2018.09.037

Smith EL, Abbott AP, Ryder KS (2014) Deep eutectic solvents (DESs) and their applications. Chem Rev 114:11060–11082. https://doi.org/10.1021/cr300162p

Spence K, Venditti R, Rojas O et al (2011) Water vapor barrier properties of coated and filled microfibrillated cellulose composite films. BioRes 6:4370–4388. https://doi.org/10.15376/biores.6.4.4370-4388

Taniguchi T, Okamura K (1998) New films produced from microfibrillated natural fibres. Polym Int 47:291–294. https://doi.org/10.1002/(SICI)1097-0126(199811)47:3%3c291::AID-PI11%3e3.0.CO;2-1

Tomé LC, Gonçalves CMB, Boaventura M et al (2011) Preparation and evaluation of the barrier properties of cellophane membranes modified with fatty acids. Carbohyd Polym 83:836–842. https://doi.org/10.1016/j.carbpol.2010.08.060

Torres JM, Stafford CM, Vogt BD (2010) Manipulation of the elastic modulus of polymers at the nanoscale: influence of UV−ozone cross-linking and plasticizer. ACS Nano 4:5357–5365. https://doi.org/10.1021/nn100720z

Wang J, Gardner DJ, Stark NM et al (2018) Moisture and oxygen barrier properties of cellulose nanomaterial-based films. ACS Sustain Chem Eng 6:49–70. https://doi.org/10.1021/acssuschemeng.7b03523

Wen Y, Yuan Z, Qu J et al (2020) Evaluation of ultraviolet light and hydrogen peroxide enhanced ozone oxidation treatment for the production of cellulose nanofibrils. ACS Sustain Chem Eng 8:2688–2697. https://doi.org/10.1021/acssuschemeng.9b06028

Yang X, Reid MS, Olsén P, Berglund LA (2020) Eco-friendly cellulose nanofibrils designed by nature: effects from preserving native state. ACS Nano 14:724–735. https://doi.org/10.1021/acsnano.9b07659

Zhang Q, De Oliveira VK, Royer S, Jérôme F (2012) Deep eutectic solvents: syntheses, properties and applications. Chem Soc Rev 41:7108. https://doi.org/10.1039/c2cs35178a